7th International Conference on Debris-Flow Hazards Mitigation

Topographic change detection at Chalk Cliffs, Colorado, USA, using airborne lidar and UAS-based Structure-from-Motion photogrammetry

Katherine R Barnhart[a,b]*, Francis K. Rengers[c], Jessica N. Ghent[d], Gregory E. Tucker[a,b], Jeffrey A. Coe[c], Jason W. Kean[c], Joel B. Smith[c], Dennis M. Staley[c], William Kleiber[e], Ashton M. Wiens[e]

[a]*University of Colorado, Department of Geological Sciences, UCB 399, Boulder, CO 80309, USA*
[b]*University of Colorado, Cooperative Institute for Research in Environmental Sciences, UCB 216, Boulder, CO 80309, USA*
[c]*U.S. Geological Survey, Landslide Hazards Group, 1711 Illinois St., Golden, CO 80401, USA*
[d]*Front Range Community College, 3645 W 112 Ave, Westminster, CO 80031, USA*
[e]*University of Colorado, Department of Applied Mathematics, UCB 526, Boulder, CO 80309, USA*

Abstract

The Chalk Cliffs debris-flow site is a small headwater catchment incised into highly fractured and hydrothermally altered quartz monzonite in a semiarid climate. Over half of the extremely steep basin is exposed bedrock. Debris flows occur multiple times per year in response to rainstorm events, typically during the summer monsoon season. The frequency of debris flows, and the uniformity of the underlying rock, make Chalk Cliffs an ideal study catchment for translating mechanistic understanding of natural debris flows to other sites. A 2008 National Center for Airborne Laser Mapping (NCALM) airborne lidar survey provides baseline topography for the site; however, heretofore there has been no systematic effort to collect repeat topography of the entire site. Starting in May 2018, we made repeat surveys of the basin with an unmanned aircraft system (UAS). The UAS-based imagery was processed into (x, y, z) point clouds using Structure-from-Motion (SfM) photogrammetry. We georegistered the point clouds using 12 ground control points placed within and around the study basin. In this study we compare the lidar with one SfM point cloud to assess topographic change over a 10-year time period. The difference map provides observational data relevant to understanding sediment provenance and transport at the Chalk Cliffs. The difference image indicates erosion of colluvial surfaces, with limited deposition in the survey area. Some colluvial hillslopes show spatially uniform erosion while others experienced concentrated erosion of up to 3 m depth over a 10-year period.

Keywords: Structure-from-Motion, topographic difference map, Chalk Cliffs

1. Introduction

Debris flows are water-laden slurries of soil and rock that move rapidly through channels in steep landscapes, and present hazards to human life, infrastructure, and property. Debris flows are among the most dangerous and frequent natural hazards—once initiated, a debris flow can continue to travel over shallow terrain, extending the hazard from steep regions to areas adjacent to the mouths of canyons and near valley bottoms. Progressive entrainment of debris through surface water runoff and bulk failure of debris are the two main mechanisms for the initiation of debris flows (Coe et al., 2008; Kean et al., 2013). Here, we apply Structure-from-Motion (SfM) to create 3D point clouds using images taken using an unmanned aircraft system (UAS). The SfM point clouds are then compared with an aerial lidar

* Corresponding author e-mail address*: katherine.barnhart@colorado.edu*

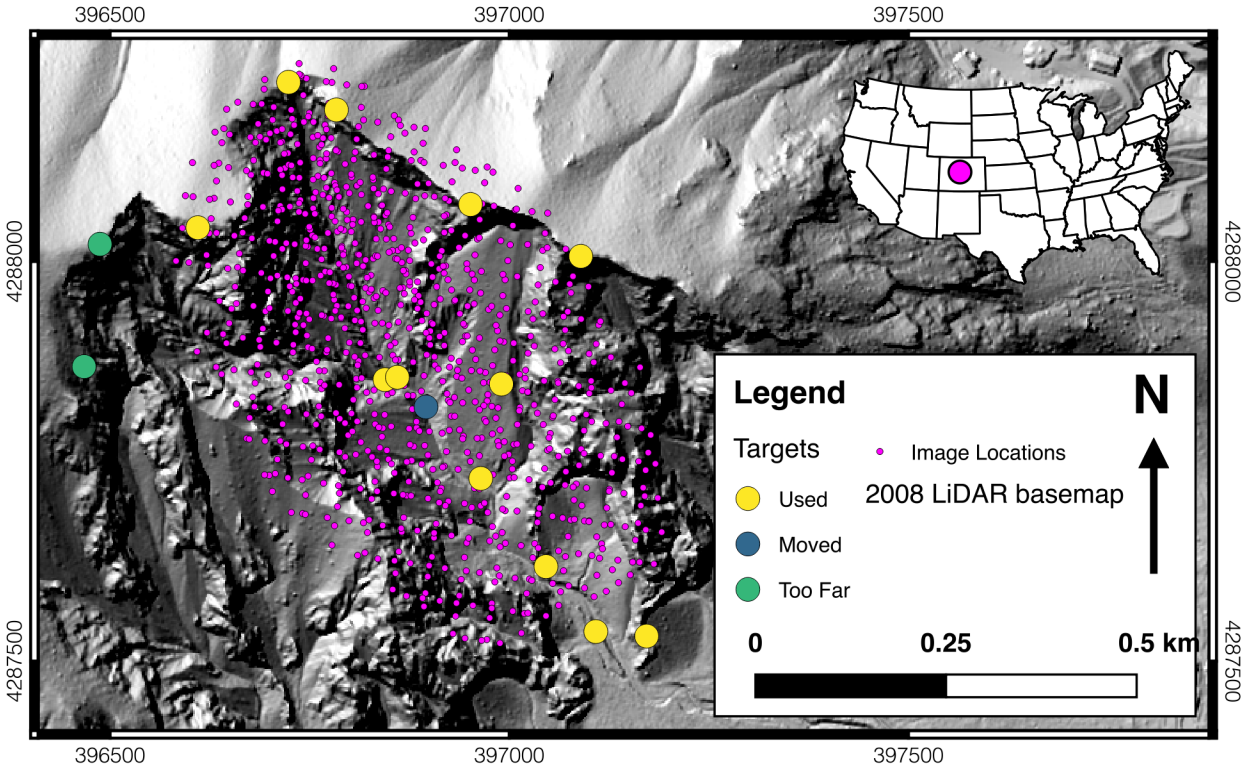

Fig 1. Field site map showing the location of ground control targets (large dots) and image locations (small dots) over the 2008 lidar basemap. The image locations are the (x, y) positions of the UAS at the time each image was taken. Map coordinate system is WGS84 UTM zone 13N.

survey (ALS) dataset taken in 2008 in order to construct a topographic difference map at a debris-flow site in central Colorado, USA.

SfM uses a set of overlapping photographs, taken from different locations, to generate 3D models without prior knowledge of image position, image look angle, or matching feature locations across image pairs (Snavely et al., 2006; 2007; 2008; James and Robson, 2012; Fonstad et al., 2013). Differencing the resulting point cloud with existing ALS provides for a topographic difference map that can be used to identify dominant geomorphic processes operating in the basin. After describing the geologic setting and the methods of data collection and processing, we describe the results of the change detection in the context of debris-flow processes.

2. Geologic Setting

The Chalk Cliffs site is a 0.37 km^2-sized drainage basin incised into highly fractured and hydrothermally altered quartz monzonite in a semiarid climate (Sharp, 1970; Coe et al., 2008). The basin is located on the southeastern corner of Mount Princeton in Colorado's Sawatch Range (Fig 1). Starting in 2004, the U.S. Geological Survey (USGS) established a monitoring site in the Chalk Cliffs basin (Coe et al., 2008). Over half of the basin is exposed bedrock, and gradients in the basin are steep—ranging from 5° to 60° in the channels, 25° to 40° on colluvial slopes, and 40° to vertical on bedrock slopes (McCoy et al., 2010). Debris flows occur one to four times per year in response to rainstorm events, usually during the summer monsoon season between May and September (Dillon and Grogger, 1982; Mortimer, 1997). An airborne lidar survey flown on October 7th, 2008, provides baseline topography (National Center for Airborne Laser Mapping, 2008). This ALS point cloud covers 55 km^2 with a total point density of 5.74 pts/m^2 and a ground point density of 3.6 pts/m^2. Additionally, there have been occasional Terrestrial Laser Scanner surveys at the site (McCoy et al., 2010; Staley et al., 2011).

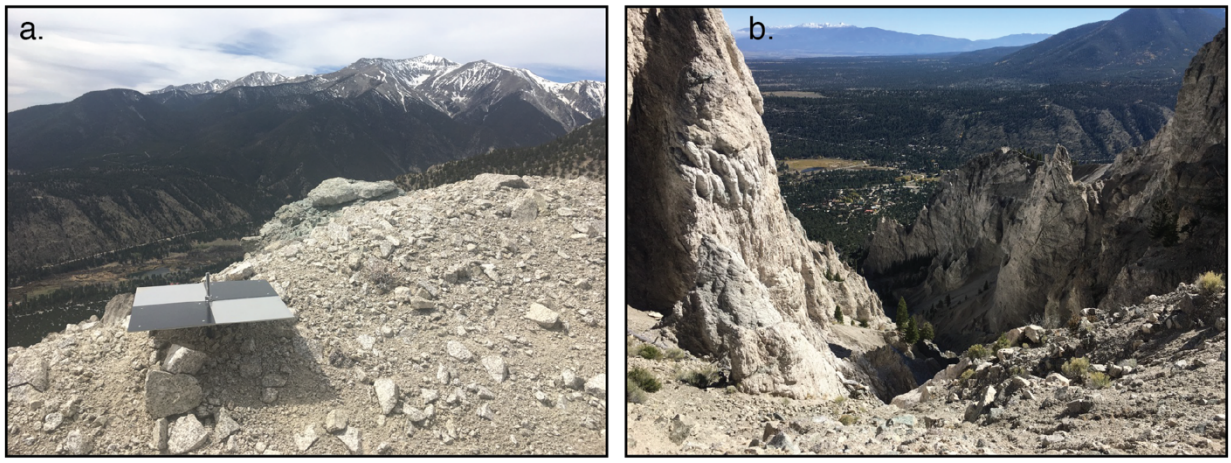

Fig 2. (a) View of ground control point (GCP) RD2 at the site. Each GCP is 16 inches square and is attached to rebar. (b) Field photo showing view of basin from UAS survey point. Photo credit for both images: Katherine Barnhart.

3. Methods

3.1. Ground Control Point Placement

In order to construct a georeferenced SfM point cloud of Chalk Cliffs, ground control points (GCPs) were required to be placed within the study basin (James and Robson, 2012). We constructed permanent GCPs (Fig 2a) and placed 15 of them in and around the study basin on May 5, 2017 (Fig 1, Table 1). The location of the center of each GCP was determined using survey-grade GPS equipment. GPS observations were processed using GNSS Solutions software by Magellan into WGS84 (G1150) latitude, longitude and ellipsoid height and UTM zone 13N easting, northing, and NAVD88 orthometric height above mean sea level (using GEOID09). Errors reported by GNSS Solutions are ±1 cm in all three directions.

3.2. Unmanned Aircraft Surveying

We undertook repeat UAS surveys of the Chalk Cliffs basin in the summer of 2018. We visited the site 10 times over this period. In this work, we only focus on the visit from June 18th. This date was chosen because it was the first set of flights to be fully processed from images to a georeferenced point cloud.

We used a DJI Phantom 4 Pro with the onboard stock camera and GPS. We programmed the mission flight paths using the MapsMadeEasy (MME) iPad software. The UAS was programmed to fly at a constant elevation above the ground surface (represented in MME by Shuttle Radar Topography Mission elevation data). The UAS was programmed to fly one multi-battery double-grid mission at 400 ft above ground level (AGL) over most of the Chalk Cliffs basin with the camera pointed at nadir and one multi-battery single-grid mission at 250 ft AGL over the interior of the eastern and southern portions basin with the camera pointed 15° off-nadir (photo locations shown in Fig 1). Flight speed and photo triggering were set to ensure 85% overlap, 80% sidelap, and motion blur of less than 0.1 pixel. The camera was set to engage autofocus only once at the beginning of each flight (above the take-off point and at cruising altitude), to take photos in RAW mode (DNG file format), and to use auto exposure settings. The number of flights necessary to accomplish the same mission depends on the wind speed during the flights. On June 18th, the basin survey required 10 flights and approximately 3 hours. The June 18th, 2018, UAS mission resulted in a total of 909 images.

We were not able to fly over the entirety of the upper western portion of the basin because it would require the UAS to fly in an area that is occluded from view from the take-off location. Even though we did not fly over the entirety of this part of the basin, tie point identification and error reduction still yielded a sufficient number of matched points to reconstruct the topography in this area. We posit that this occurred because of the high level of overlap and side lap used in the UAS survey plan.

Table 1. Location of ground control points at study site.

Point Name	UTM zone 13N Easting (m)	UTM Zone 13N Northing (m)	Orthometric (NAVD88) Height above mean sea level (m)	WGS84 Longitude	WGS84 Latitude	Ellipsoid Height (m)	Comments
T3	396844.354	4287852.198	2777.991	106° 11' 12.57469"	38° 43' 59.95738"	2763.751	Used
T4	396859.901	4287855.177	2773.339	106° 11' 11.93252"	38° 44' 00.06053"	2759.098	Used
T9	396895.794	4287817.972	2759.541	106° 11' 10.42620"	38° 43' 58.86887"	2745.299	Moved
DT1	397172.146	4287531.326	2685.091	106° 10' 58.82899"	38° 43' 49.68735"	2670.836	Used
DT2	397108.508	4287537.005	2673.035	106° 11' 01.46722"	38° 43' 49.84486"	2658.782	Used
DT3	397046.074	4287618.310	2697.428	106° 11' 04.09608"	38° 43' 52.45583"	2683.178	Used
DT4	396964.370	4287728.544	2726.193	106° 11' 07.53850"	38° 43' 55.99704"	2711.947	Used
DT5	396990.221	4287846.686	2807.117	106° 11' 06.53131"	38° 43' 59.83986"	2792.872	Used
RD1	397089.690	4288006.511	3050.903	106° 11' 02.49786"	38° 44' 05.06562"	3036.657	Used
RD2	396951.457	4288071.344	3052.344	106° 11' 08.25705"	38° 44' 07.11047"	3038.103	Used
RD3	396783.498	4288189.678	3042.692	106° 11' 15.27604"	38° 44' 10.87807"	3028.458	Used
RD4	396723.543	4288224.254	3026.432	106° 11' 17.77750"	38° 44' 11.97431"	3012.200	Used
RD5	396609.904	4288042.318	3142.828	106° 11' 22.38566"	38° 44' 06.02529"	3128.597	Used
RD6	396487.367	4288021.633	3165.115	106° 11' 27.44894"	38° 44' 05.30268"	3150.888	Too Far
RD7	396467.437	4287868.513	3093.844	106° 11' 28.19178"	38° 44' 00.32779"	3079.616	Too Far

3.3. Structure-From-Motion Photogrammetry Processing

All 909 photos were imported into Agisoft PhotoScan Pro (version 1.4.3). Images were imported in RAW format and no image preprocessing was done. Image quality was checked using Photoscan, and images with quality values of less than 0.7 were discarded. The remaining 899 photos were aligned with settings of 60,000 key points, 0 tie points (which means all are kept), highest accuracy, generic preselection, and reference preselection. Adaptive camera model fitting was turned off. This resulted in the creation of 3.4 million tie points. We then performed the first two of three steps of gradual selection on the tie points: reconstruction uncertainty and projection accuracy. In this process, we followed the recommendations of the USGS National Unmanned Aircraft Systems Project Office (National Unmanned Aircraft Systems Project Office, 2017) developed in collaboration with Tom Noble (Breithaupt et al., 2004; Thoeni et al., 2014; Matthews et al., 2016; Warrick et al., 2017; Sherwood et al., 2018, Noble, *oral communication, 2018*).

The first step, reconstruction uncertainty, removes tie points with poor geometry. We removed tie points with a reconstruction uncertainty value of 15 or above and then re-ran camera optimization. Note that none of the gradual selection metric values have units. In the second step, we removed tie points with bad projection accuracy (values above 3) associated with tie points with pixel matching errors. After the first two steps of gradual selection, the locations of the GCP targets were imported into PhotoScan. We used the WGS84 zone 13 N UTM easting and northing and the WGS84 ellipsoidal height as the reference frame. Each of the 13 used targets were hand-marked in each of the photographs. We estimated a marker placement uncertainty of 0.1 pixels. After the markers were placed, we performed the final step of gradual selection: reprojection error. In this step, tie points that have bad pixel residual errors are removed. We removed points down to a reprojection error level of 0.3. At the end of gradual selection, the original 3.4 million tie points were reduced to a set of 1.2 million. Even though we had not flown over the entirety of the western portion of the basin, we were able to get sufficient tie points with good characteristics to reconstruct the topography in much of this area.

We explored how increasing the number of GCPs influenced the check point root mean squared error (RMSE) by undertaking the error reduction process for multiple sets of GCPs. We found that the check point RMSE (1σ) of our results was 4 cm. This magnitude is similar to that identified in similar studies (Warrick et al., 2017).

Finally, we built a dense cloud on the medium quality setting and exported it as a LAZ file. This created a point cloud with 47 million points each of which have an (x, y, z) as well as red, blue, and green (RGB) color attributes (Fig 3b). The RGB color is based on the pixel values of the original images. The point cloud covers an area of ~0.75 km^2 and has a point density of ~70 pts/m^2.

3.4. Lidar point cloud reprojection

The ALS point cloud has a horizontal reference system of NAD83 UTM zone 13N and a vertical reference system of NAVD88 based on GEOD03. To perform change detection between the ALS and the SfM point cloud, we converted the ALS dataset to the SfM point cloud reference frame. We used NOAA's VDATUM program to convert the lidar to WGS84 (G1150) UTM zone 13N horizontal reference frame and the WGS84 (G1150) ellipsoidal height vertical reference frame.

3.5. SfM point cloud tree removal

SfM point clouds are based on optical imagery, and thus they create (x, y, z) points that represent the surface of trees in the surveyed area. Unlike lidar, SfM does not see *through* trees and there are no "ground" points within the footprint of each tree. Thus, we needed a suitable approach for the separation of "ground" and "tree" point returns in the SfM point cloud. We determined RGB and whole-point cloud-based classification methods to be insufficient to differentiate between shady rock crevices and trees. As an alternative, we identified the following method, which was successful at removing trees from the SfM point cloud. Starting with the entire 2008 ALS dataset (all returns), we reset the "ground/other" classification and reclassified points into ground/vegetation/unclassified using LAStools (LAStools, 2018). We then examined all the vegetation points in the context of the SfM cloud and manually added additional points where the SfM point cloud shows that a tree is present, but the lidar has no vegetation points. The x and y coordinates of this "tree-only" point cloud were then buffered by 3.5 m and merged in order to create the tree mask shown in Fig 3a. We tried smaller buffer sizes but found that 3.5 m was the minimum distance required to remove the trees. Finally, we removed all points from the SfM cloud that had (x, y) coordinates within the tree mask. Areas covered by the tree mask were not considered in the change detection analysis.

3.6. Difference Construction

Next, we performed a change detection analysis between the tree-removed SfM cloud with the ground-only version of the 2008 lidar available through OpenTopography using the Multiscale Model to Model Cloud Comparison (M3C2) plugin in CloudCompare (Lague et al., 2013). This approach is suitable for comparing two point clouds, particularly when they have different point densities. As the lidar has a ground point density of 3.6 pts/m^2 and the SfM cloud has a density of ~70 pts/m^2, we used all of the lidar ground points as the core points for M3C2. We used a value of 3 m for the projection scales, a max depth of 30 m, and multi-scale calculation of the normal (min=1, step=0.5, max=5 m). We estimate our limit of detection (LoD) as the independent combination of normally distributed uncertainties in the SfM point cloud (1σ=5 cm), the ALS (1σ=10 cm), and the GCP locations (1σ=1 cm). This yields a combined 1σ LoD of 11 cm. Plan-view and perspective views of the M3C2 distance are presented in Fig 3.

3.7. Calculation of basin-averaged erosion rate

We estimated the basin-averaged erosion rate by exporting the M3C2 difference point cloud from CloudCompare to a GeoTIFF raster at a horizontal scale of 1 m. After clipping the M3C2 difference to area inside the basin, we calculate an average erosion depth of 0.02 m over the 10-year baseline. Given the basin area of 0.37 km^3, this average erosion depth corresponds to an average volumetric sediment export of 750 m^3 per year.

4. Results and Discussion

The results of the October 2008–June 2018 lidar-SfM topographic difference highlight active geomorphic processes. In many areas of the basin, the difference image indicates up to 3 m of erosion (Figs 3 and 4). Given the RMSE of ~10 cm, we cannot expect to resolve centimeter-scale changes in elevation; however, much of the basin has experienced topographic change in excess of our detection limit. Therefore, we have focused on changes to the colluvial regions of the study area.

There are three main types of colluvial surfaces within the surveyed area. First are surfaces that have not eroded or aggraded at levels beyond our limit of detection over the ten-year period. Many of these surfaces (such as the one

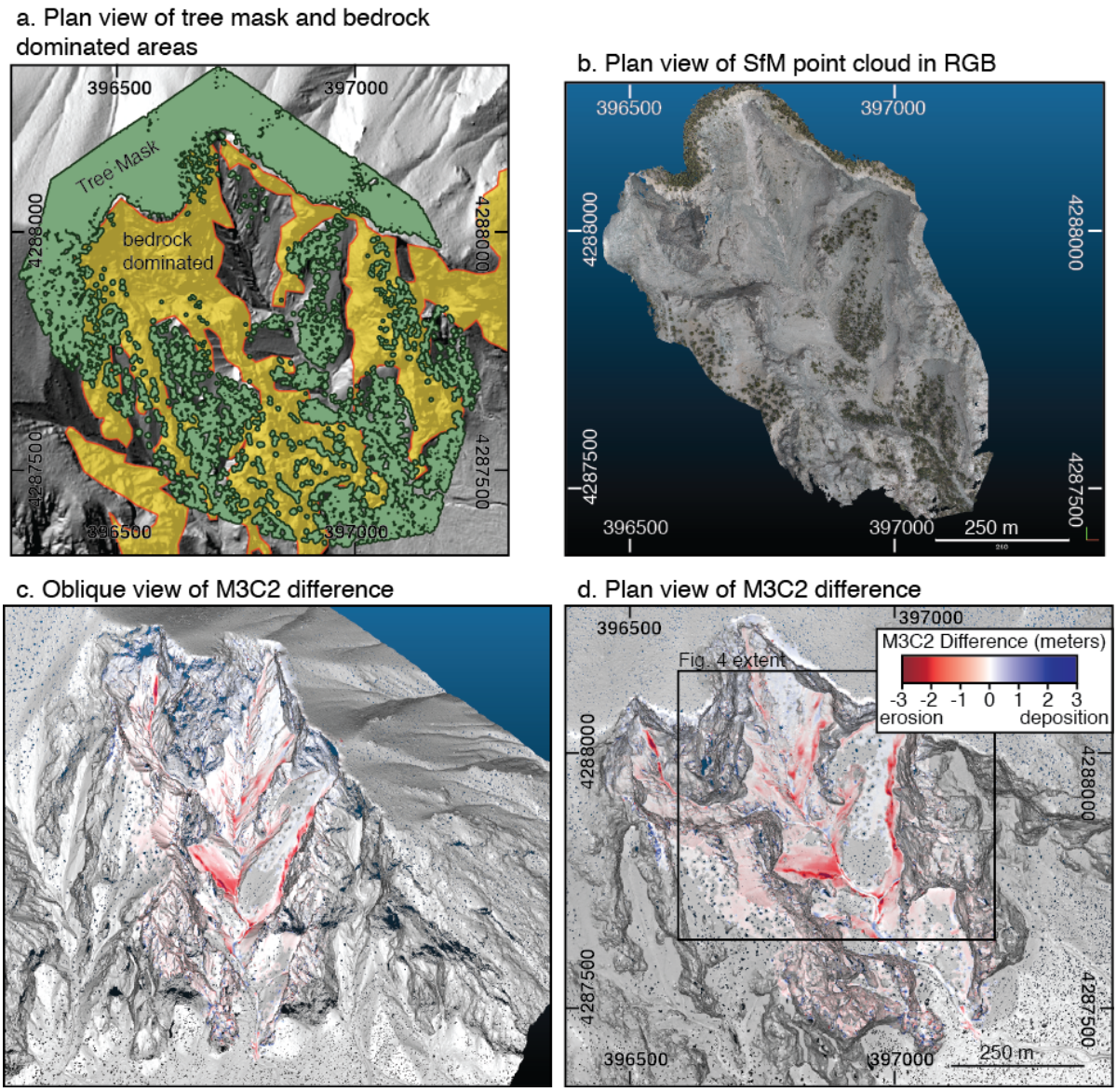

Fig 3. Results of SfM construction and M3C2 differencing. Shaded relief map derived from 2008 ALS. (a) shows the tree mask (green) and the areas dominated by bedrock (yellow). Areas with no color in (a) are neither tree covered nor dominated by bedrock. Areas covered by the tree mask were excluded from the change detection analysis. (b) and (d) show look down views of the basin in true-color (RGB) and as a shaded relief with M3C2 difference overlain, respectively. (c) shows a perspective view of the basin. The extent of Fig 4 shown in panel d.

labeled "stable colluvial surface" in Fig 4) are tree covered—where the trees are present, we are not able to assess topographic change. However, away from trees, the estimated topographic difference on this surface is within ±11 cm (below our LoD). Second are colluvial surfaces above the main cliff band, which have eroded slightly (0.2-0.3 m of erosion) and relatively uniformly. The stable colluvial surface labeled in Fig 4 has a slope of ~34° while the slope above the cliff band is slightly steeper (~36°). The final type of colluvial surface has spatially variable erosion likely due to erosion by concentrated surface runoff. Fig 4 shows two examples of this sort of surface: the margins of the stable colluvial surface, and the surface labeled "A." The pattern of erosion in this second example of an eroding surface is shown as an example of "firehose impact" erosion described by Coe et al. (2008, their Fig 9).

In both channels in the upper portion of the study basin, it appears that erosion of the channel has occurred. The condition of the beds of these channels during the lidar flight is unknown, making estimation of channel bedrock lowering difficult. Thus, we are unable to determine how much of the ~3 m of erosion in the upper west part of the channel is due to the evacuation of sediment, the erosion of bedrock, and the plucking of large blocks. The channel

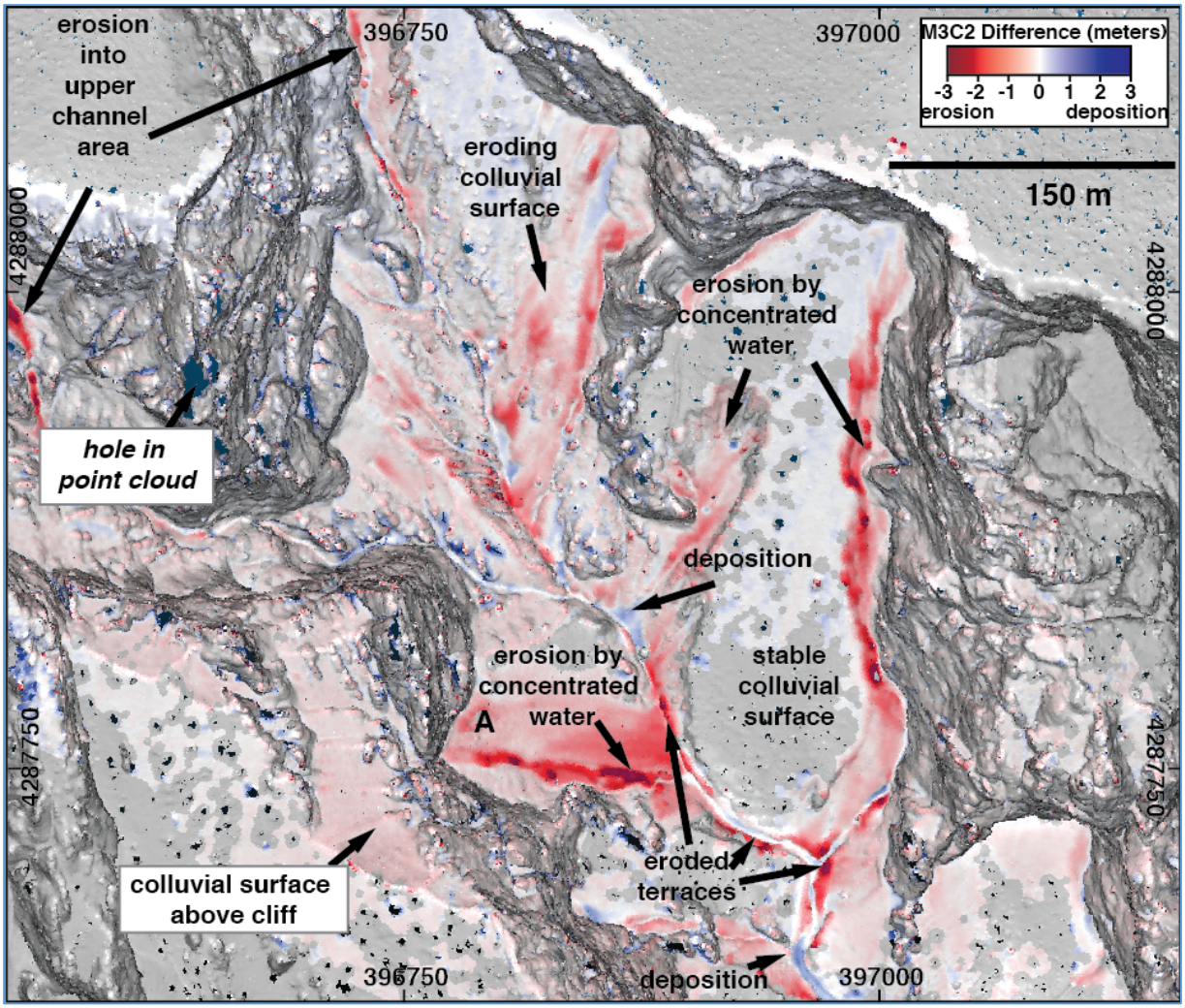

Fig 4. Shaded relief map of the site colored by M3C2 difference and annotated with features in the difference map.

thalweg has been observed in the field to alternate between periods when bedrock is exposed (commonly after debris flows), and periods when the channel is filled with sediment (between debris flows). Elsewhere in the basin, the channel shows patterns of erosion, no change, and deposition. Deposition may be associated with areas of temporary sediment storage in lower-gradient channel segments (Kean et al., 2013). Elsewhere in the basin there is extensive erosion of the terraces adjacent to the channels.

5. Conclusions

Here, we have demonstrated that SfM and lidar can be used in combination to identify topographic change over a 10-year period at an active debris-flow site. Patterns of topographic change in the Chalk Cliffs basin are dominated by erosion of colluvial surfaces. The combined geomorphic processes yield a basin-averaged erosion rate of 0.002 m per year and a sediment export rate of 750 m^3 per year. Along the channel thalweg, we are unable to attribute topographic change to specific geomorphic process. Comparing two SfM point clouds, each with extensive optical imagery, will be able to pinpoint the evolution of sediment coverage within the channel thalweg.

Acknowledgements

KRB was supported by NSF Grant EAR-1725774. JNG was supported during a Research Experience for Community College Students internship by NSF-EAR 1757930 and by NSF EAR-1450409 (to GET). Additional funding for this work was provided by a University of Colorado Innovative Seed Grant Program proposal to WK. KRB thanks Rachel Glade, Charlie Shobe, Matt Rossi, Robert Anderson, Nadine Reitman, Charlie Shobe, and Margaux Mouchene for assistance in the field, Tom Noble and Chris Sherwood for help with Agisoft PhotoScan best practices, and Frontier Ranch Young Life Camp for access to the site through their property. The lidar data were accessed through OpenTopography. Lidar data acquisition and processing completed by the National Center for Airborne Laser Mapping (NCALM - http://www.ncalm.org). NCALM funding provided by NSF's Division of Earth Sciences, Instrumentation and Facilities Program. EAR-1043051. We thank the editors, one anonymous reviewer, and Erin Bessette-Kirton for comments that improved the quality of the manuscript. Any use of trade, firm, or product names is for descriptive purposes only and does not imply endorsement by the U.S. Government.

References

CloudCompare (version 2.9.1) [GPL software]. (2018). Retrieved from http://www.cloudcompare.org/

Breithaupt, B.H., Matthews, N.A., and Noble, T.A., 2004, An Integrated Approach to Three-Dimensional Data Collection at Dinosaur Tracksites in the Rocky Mountain West: Ichnos, v. 11, p. 11–26, doi: 10.1080/10420940490442296.

Coe, J.A., Kinner, D.A., and Godt, J.W., 2008, Initiation conditions for debris flows generated by runoff at Chalk Cliffs, central Colorado: Geomorphology, v. 96, p. 270–297, doi: 10.1016/j.geomorph.2007.03.017.

Dillon, G.D., and Grogger, P.K., 1982, Mudflows of Mt. Princeton/Chalk Creek, Chaffee County, Colorado: Geological Society of America Abstracts with Programs 14 (6) 309.

Fonstad, M.A., Dietrich, J.T., Courville, B.C., Jensen, J.L., and Carbonneau, P.E., 2013, Topographic structure from motion: a new development in photogrammetric measurement: Earth Surface Processes and Landforms, v. 38, p. 421–430, doi: 10.1002/esp.3366.

James, M.R., and Robson, S., 2012, Straightforward reconstruction of 3D surfaces and topography with a camera: Accuracy and geoscience application: Journal of Geophysical Research, v. 117, p. F03017, doi: 10.1029/2011JF002289.

Kean, J.W., McCoy, S.W., Tucker, G.E., Staley, D.M., and Coe, J.A., 2013, Runoff-generated debris flows: Observations and modeling of surge initiation, magnitude, and frequency: Journal of Geophysical Research-Earth Surface, v. 118, p. 2190–2207, doi: 10.1002/jgrf.20148.

Lague, D., Brodu, N., and Leroux, J., 2013, Accurate 3D comparison of complex topography with terrestrial laser scanner: Application to the Rangitikei Canyon (NZ): ISPRS Journal of Photogrammetry and Remote Sensing, v. 82, p. 10–26, doi: 10.1016/j.isprsjprs.2013.04.009.

LAStools, (2018) "Efficient LiDAR Processing Software", obtained from http://rapidlasso.com/LAStools October 2018.

Matthews, N., Noble, T.A., and Breithaupt, B.H., 2016, Close-Range photogrammetry for 3D ichnology: the basics of photogrammetric ichnology, *in* Falkingham, P.L., Marty, D., and Richter, A. eds., Dinosaur tracks-Next Steps, Bloomington, Indiana University Press, p. 29–55.

McCoy, S.W., Kean, J.W., Coe, J.A., Staley, D.M., Wasklewicz, T.A., and Tucker, G.E., 2010, Evolution of a natural debris flow: In situ measurements of flow dynamics, video imagery, and terrestrial laser scanning: Geology, v. 38, p. 735–738.

Mortimer, P., 1997, Stratigraphic and rheologic analysis of debris flow deposits in Chalk Creek Canyon, Colorado. Thesis for distinction in Geology, Colorado College, 99 p.

National Center for Airborne Laser Mapping, 2008, San Isabel NF, CO: Debris Flow Mechanics and Landscape Evolution, doi: 10.5069/G9TX3C9D.

National Unmanned Aircraft Systems Project Office, 2017, Unmanned Aircraft Systems Data Post - Processing Structure - Photogrammetry from - Motion, p. 1–21, https://uas.usgs.gov/pdf/PhotoScanProcessingDSLRMar2017.pdf.

Sharp, W.N., 1970, Extensive zeolitization associated with hot springs in central Colorado: U.S. Geological Survey Professional Paper 700-B, p. B14–B20.

Sherwood, C.R., Warrick, J.A., Hill, A.D., Ritchie, A.C., Andrews, B.D., and Plant, N.G., 2018, Rapid, Remote Assessment of Hurricane Matthew Impacts Using Four-Dimensional Structure-from-Motion Photogrammetry: Journal of Coastal Research, v. 346, p. 1303–1316, doi: 10.2112/JCOASTRES-D-18-00016.1.

Snavely, N., Garg, R., Seitz, S.M., and Szeliski, R., 2008, Finding paths through the world's photos: ACM Transactions on Graphics (TOG), v. 27, p. 15, doi: 10.1145/1399504.1360614.

Snavely, N., Seitz, S.M., and Szeliski, R., 2007, Modeling the World from Internet Photo Collections: International Journal of Computer Vision, v. 80, p. 189–210, doi: 10.1007/s11263-007-0107-3.

Snavely, N., Seitz, S.M., and Szeliski, R., 2006, Photo tourism: exploring photo collections in 3D: ACM, exploring photo collections in 3D, v. 25, p. 835–846, doi: 10.1145/1141911.1141964.

Staley, D.M., Wasklewicz, T.A., Coe, J.A., Kean, J.W., McCoy, S.W., and Tucker, G.E., 2011, Observations of debris flows at Chalk Cliffs, Colorado, USA: Part 2, Changes in surface morphometry from terrestrial laser scanning in the summer of 2009 (R. Genevois, D. L. Hamilton, & A. Prestininzi, Eds.): Debris-flow Hazards Mitigation, Mechanics, Prediction, and Assessment, p. 759–768, doi: 10.4408/IJEGE.2011-03.B-083.

Thoeni, K., Giacomini, A., Murtagh, R., and Kniest, E., 2014, A comparison of multi-view 3D reconstruction of a rock wall using several cameras and a laser scanner: Proceedings of the International Archives of the Photogrammetry, Remote Sensing and Spatial Information Sciences 2014 ISPRS Technical Commission V Symposium, v. XL-5, p. 573–580.

Warrick, J.A., Ritchie, A.C., Adelman, G., Adelman, K., and Limber, P.W., 2017, New Techniques to Measure Cliff Change from Historical Oblique Aerial Photographs and Structure-from-Motion Photogrammetry: Journal of Coastal Research, v. 331, p. 39–55, doi: 10.2112/JCOASTRES-D-16-00095.1.